文章编号: 1000-324X(2023)09-1005-12 **DOI:** 10.15541/jim20230132

卤化物钙钛矿光电阻变机理研究进展

郭华军[1,2], 安帅领[2,3], 孟 婕[2,3], 任书霞[3], 王文文[2],
梁子尚[1,2], 宋佳钰[2,3], 陈恒彬[2,3], 苏 航[2,3], 赵晋津[2]

(1. 石家庄铁道大学 机械工程学院, 石家庄 050043; 2. 河北师范大学 化学与材料科学学院, 河北省无机纳米材料重点实验室, 石家庄 050024; 3. 石家庄铁道大学 材料科学与工程学院, 石家庄 050043)

摘 要: 阻变器作为一种基于可逆、非易失、阻态突变的信息存储和处理器件, 是解决传统存储器的内在物理限制和冯·诺依曼架构瓶颈问题的核心电子元器件之一, 受到了广泛关注。卤化物钙钛矿具有快速的载流子迁移特性和优异的光电转换性能, 作为阻变功能层赋予光电阻变存储器优异的阻变性能。因此, 近年来卤化物钙钛矿基阻变器的存储和计算应用研究发展迅速。然而, 目前对于卤化物钙钛矿的光电阻变机理尚未形成统一认识。基于此, 本文分析了卤化物钙钛矿阻变存储器的工作机理, 对比分析了卤化物钙钛矿基光电阻变器导电细丝和能级匹配调控特性, 总结了其各种机理的制约因素, 揭示了导电细丝在光场和电场作用下重复形成和断裂, 以及阻变器中卤化物钙钛矿功能层和其他功能层之间肖特基势垒改变, 主导卤化物钙钛矿光电阻变器的开关比、阈值(Set/Reset)电压和阻变器性能稳定性, 并进一步展望卤化物钙钛矿基光电阻变器在新型人工智能仿生突触、存内运算、机器视觉的应用。

关 键 词: 导电细丝; 能级匹配; 卤化物钙钛矿; 存内运算; 机器视觉; 综述

中图分类号: TM546 **文献标志码:** A

Research Progress of Photoelectric Resistive Switching Mechanism of Halide Perovskite

GUO Huajun[1,2], AN Shuailing[2,3], MENG Jie[2,3], REN Shuxia[3], WANG Wenwen[2],
LIANG Zishang[1,2], SONG Jiayu[2,3], CHEN Hengbin[2,3], SU Hang[2,3], ZHAO Jinjin[2]

(1. School of Mechanical Engineering, Shijiazhuang Tiedao University, Shijiazhuang 050043, China; 2. Hebei Key Laboratory of Inorganic Nano-materials, College of Chemistry and Materials Science, Hebei Normal University, Shijiazhuang 050024, China; 3. School of Materials Science and Engineering, Shijiazhuang Tiedao University, Shijiazhuang 050043, China)

Abstract: As a reversible, non-volatile, and resistive state mutation information storage and processing device, the resistive switching (RS) memory is expected to solve the inherent physical limitations of the traditional memory and

收稿日期: 2023-03-16; **收到修改稿日期:** 2023-05-23; **网络出版日期:** 2023-06-15

基金项目: 国家自然科学基金(U2130128, 11772207); 河北省教育厅自然科学基金(ZD2020192); 河北省市场监管局科技计划(2023ZC03); 中央引导地方科技发展资金(216Z4302G); 河北省创新能力提升计划(22567604H); 京津冀基础研究合作专项(H2022205047, 22JCZXJC00060, E3B33911DF); 河北师范大学博士科研启动基金(L2023B18)
National Natural Science Foundation of China (U2130128, 11772207); Natural Science Foundation of Hebei Education Department (ZD2020192); Hebei Administration for Market Supervision Science and Technology Project List (2023ZC03); Central Government Guiding Local Science and Technology Development Project (216Z4302G); Innovation Capability Improvement Plan Project of Hebei Province (22567604H); Basic Research Cooperation Special Foundation of Beijing-Tianjin-Hebei Region (H2022205047, 22JCZXJC00060, E3B33911DF); Ph.D Scientific Research Start-up Fund of Hebei Normal University (L2023B18)

作者简介: 郭华军(1983–), 男, 博士研究生. E-mail: ghjfriend@foxmail.com
GUO Huajun (1983–), male, PhD candidate. E-mail: ghjfriend@foxmail.com

通信作者: 赵晋津, 教授. E-mail: jinjinzhao2012@163.com
ZHAO Jinjin, professor. E-mail: jinjinzhao2012@163.com

von Neumann bottleneck, and has received widespread attention. Taking advantage of rapid carrier migration characteristics and excellent photoelectric conversion performance, halide perovskite optoelectronic RS memory devices present excellent resistive switching performance. In recent years, researches on storage and computing applications of the halide perovskite RS memory developed unprecedentedly; whereas, the working mechanisms of halide perovskite RS memory still remain unclear. This review analyzes the working mechanism of halide perovskite RS memory, compares the regulation characteristics of conduction filaments (CFs) and energy level matching (ELM), summarizes the constraints of various mechanisms, reveals the repeated formation and dissolution of CFs under light illumination and electric field, as well as Schottky barrier between the perovskite transfer layer and other layer, dominates the On/Off ratio, threshold (Set/Reset) voltage and performance stability of halide perovskite optoelectronic RS memory, and prospects the applications of halide perovskite RS memory in artificial intelligence bionic synapses, in-memory computing, and machine vision.

Key words: conductive filament; energy level matching; halide perovskite; in-memory computing; machine vision; review

随着人工智能(AI)和物联网(IoT)飞速发展，当今海量的数据信息对存储技术提出了越来越高的要求。传统信息处理器将计算和存储功能分开，大数据传输势必导致冯·诺依曼瓶颈问题越来越严重[1-2]。阻变器(RRAM)是在高阻态(HRS)/低阻态(LRS)之间实现可逆转换的非易失性信息存储和信息处理器件[3-7]，有望解决传统存储器的内在物理限制并突破冯·诺依曼架构的瓶颈[8]。1971 年，Chua[9]制备的阻变器以电流-电压曲线迟滞回路为特征，通过电荷控制实现电阻转变[10-11]。卤化物钙钛矿是近年重要的光电材料，其离子迁移特性是可以实现阻变存储和仿生突触行为的重要原因之一[12-13]。Yoo 等[14]首先报道了 Au/$CH_3NH_3PbI_{3-x}Cl_x$/FTO(FTO: fluorine-doped tin oxide)结构的卤化物钙钛矿阻变器，在低于 1 V 的工作电压下，展示出典型的双极阻变行为，具有优异的非易失均匀性和稳定性。除此之外，光信号调控卤化物钙钛矿阻变器性能也得到了广泛研究[15-18]，如近期本课题组研究报道了新颖的 $CsPbBr_3$ 量子点混合氧化石墨烯柔性阻变器，实现了优异的光电双控阻变性能[19]。当前仿生突触钙钛矿器件研究[20-21]，无铅钙钛矿阻变器研究[22-23]等研究领域受到广泛关注，但是对三维(3D)、二维(2D)卤化物钙钛矿阻变器导电细丝和能级匹配机理研究尚未形成统一认识。本文系统总结了各种导电细丝机理和能级匹配对卤化物钙钛矿阻变器性能的影响。卤化物钙钛矿基光电阻变器微观机理与应用，如图 1 所示。通过调控阻变器中钙钛矿层导电细丝的形成，缩小钙钛矿与相邻层界面势垒的高度差，使器件转变为低阻态；反之断裂导电细丝，增大势垒高度可以使器件恢复高阻态[18]。

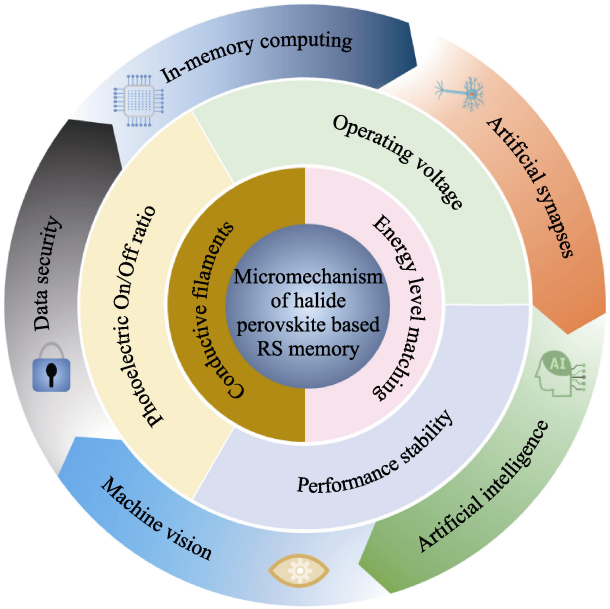

图 1 卤化物钙钛矿阻变器的机理及其应用

Fig. 1 Schematic diagram of mechanisms and applications of halide perovskite RS devices

电场和光场信号可以调控阻态转变，进而模拟仿生突触、实现数据存储以及逻辑运算功能，如 $Cs_2AgSbBr_6$ 基阻变仿生器、丙基吡啶碘化铅(PrPyr[PbI_3])基阻变器交叉系统、$CsBi_3I_{10}$ 钙钛矿/碳纳米管基光电器件等，在仿生模拟、存内运算、系统安全等领域展示出巨大的应用潜能[24-26]。

本文内容主要分为三部分：第一部分讨论卤化物钙钛矿基光电阻变器的导电细丝阻变机理；第二部分讨论卤化物钙钛矿基光电阻变器的能级匹配导致的界面势垒对阻变性能的影响；第三部分介绍卤化物钙钛矿基器件的阻变特性在仿生突触、数据存储及逻辑运算等领域的应用。

1　导电细丝

卤化物钙钛矿阻变器结构示意图，如图 2(a)所示，一般包括金属顶电极、卤化物钙钛矿阻变功能层和底电极[27]。导电细丝一般分为金属型[28-32]、卤素空位型[33-37]与杂化型导电细丝[19,38-39]，这些细丝的形成和断裂是阻变器传导的重要机制。本文从三维结构和二维结构钙钛矿阻变机理出发，研究导电细丝工作机理。

1.1　三维结构钙钛矿导电细丝机理

三维结构(3D)卤化物钙钛矿具有共用 BX_6 八面体六个卤素顶点的结构，使其在阻变器中具有广泛的应用前景[40]。图 2(b, c)展示了卤化物钙钛矿基阻变器典型的双极性阻变行为[41]，On/Off 机理为卤素空位和金属离子在卤化物钙钛矿功能层中的迁移导致器件导电细丝形成和断裂，从而触发阻变器阻态的

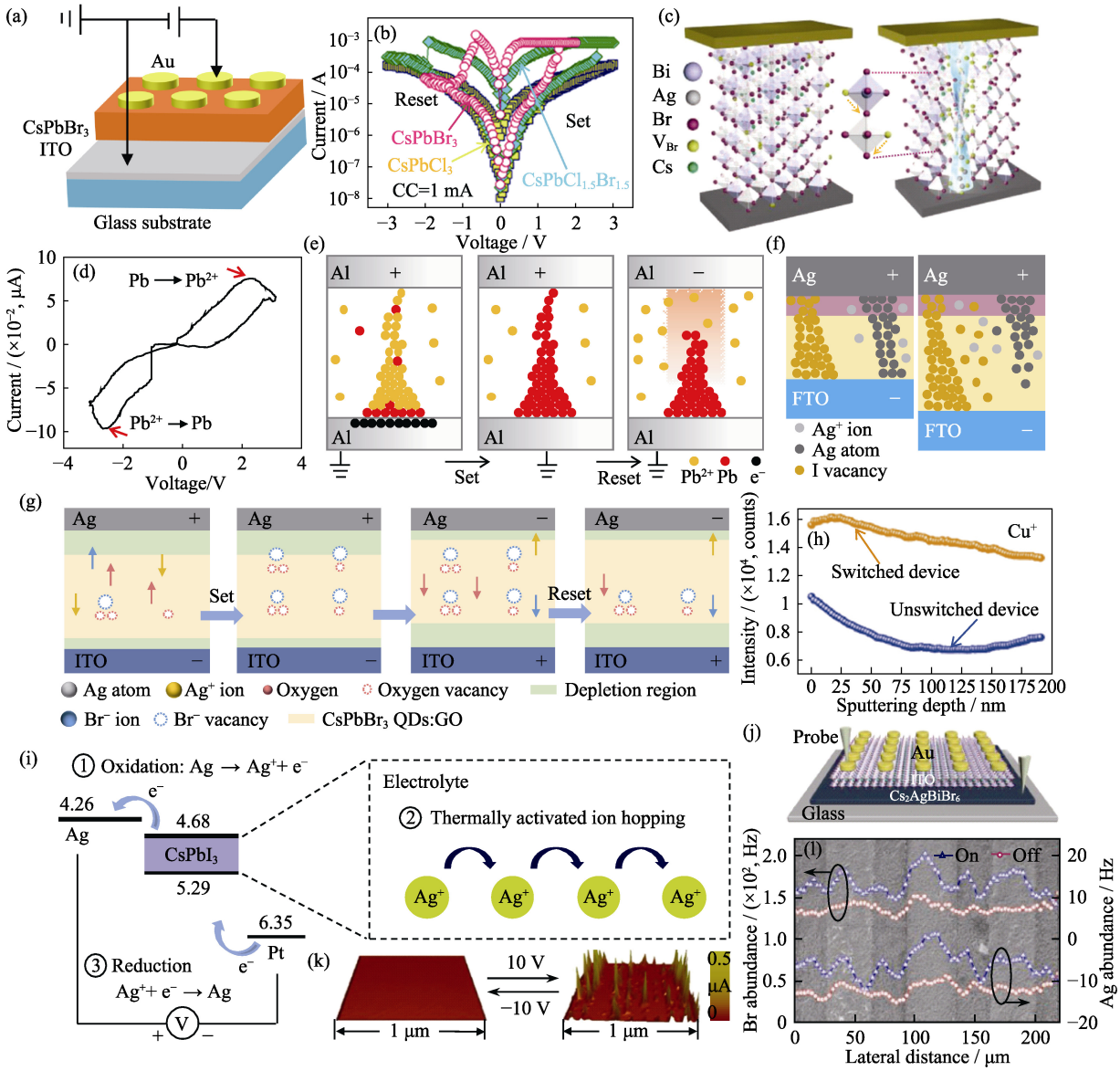

图 2　3D 钙钛矿阻变器的导电细丝[19,27,30-32,37,41-42]

Fig. 2　CFs of 3D perovskite RS device[19,27,30-32,37,41-42]

(a) Illustration of Au/$CsPbBr_3$/ITO RS device structure[27]; (b) *I*–*V* response of Al/$CsPbCl_xBr_{3-x}$/ITO/PET RS device in semilogarithmic scale[41]; (c) Alignment of bromide vacancies and silver atoms in On state of ITO/$Cs_2AgBiBr_6$/Au RS device[42]; (d) Pb element oxidation and reduction peaks at cyclic voltammetry (CV) curve of Al@$MAPbI_3$/Al; (e) Pb metallic filaments formation in Set process and dissolution in the Reset process[30]; (f) Perovskite thickness-dependent competition between metallic and iodine vacancy CFs of Ag/$MAPbI_3$/FTO RS device[37]; (g) Hybrid filaments formation and dissolution of Ag/$CsPbBr_3$ QDs:GO/ITO device[19]; (h) Intensity of Cu element on switched and unswitched Cu/$MA_3Bi_2I_9$/ITO devices[31]; (i) Band diagram of Ag/PMMA/$CsPbI_3$/Pt device and thermally activated Ag ions hopping in $CsPbI_3$[32]; (j) Schematic diagram of ITO/$Cs_2AgBiBr_6$/Au RS device; (k) Atomic force microscope images of CFs in Off (left) and On (right) states of Fig 2(j); (l) Element distributions of Br and Ag in Off and On states in Fig 2(j)[42]. ITO: Indium-tin oxide; PET: Polyethylene terephthalate; MA: Methylammonium; QDs: Quantum dots; GO: Graphene oxide; PMMA: Poly(methylmethacrylate)

开关转变[42]。

阻变器电极金属以及卤化物钙钛矿中的金属元素和卤素元素迁移都会形成导电细丝, 实现器件阻态转变。如纤维交叉阻变器 Al@$CH_3NH_3PbI_3$ ($MAPbI_3$)/Al 循环伏安曲线(图 2(d))的氧化还原峰, 对应于 Pb^{2+} 与 Pb^0 之间的氧化还原转变, 即施加正向电压时, $MAPbI_3$ 中大量 Pb^{2+}向负极移动, 并且 Pb^{2+}在负极被电子还原为 Pb 原子, 当电压增大到写入(Set)电压时, Pb 原子组成的金属导电细丝连通正负极, 器件转变为低阻态。当给器件施加反向电压扫描, 电压达到复位(Reset)电压时, 辅助焦耳热导致 $MAPbI_3$ 中铅金属导电细丝断裂, 器件由低阻态转变为高阻态[30], 如图 2(e)所示。除了钙钛矿 B 位金属形成导电细丝, 钙钛矿层的 X 位卤素也会参与导电细丝的形成。图 2(f)展示了碘空位($V_I^{\cdot}$)和 Ag 金属导电细丝的竞争行为。$MAPbI_3$ 厚度较大时, 施加 Set 电压后，仅 I^- 迁移形成了连通正负电极的 $V_I^{\cdot}$ 导电细丝; $MAPbI_3$ 厚度显著减小时, 施加 Set 电压可以形成 $V_I^{\cdot}$和 Ag 金属导电细丝并联, 连通正负电极, 由于 Ag 导电细丝电阻比 $V_I^{\cdot}$ 导电细丝小一个数量级[43], 此时的低阻态电阻由 Ag 金属导电细丝主导[37]。其它材料(如石墨烯)掺杂的钙钛矿材料的阻变器中, X 位卤素空位及掺杂元素空位共同参与杂化导电细丝的形成。如 Ag/$CsPbBr_3$ QDs: GO/ ITO 器件(图 2(g))随着正电压增大, Ag 电极的 Ag 原子氧化为 Ag^+, 并在电压驱使下向器件负极移动, 在负极积累且还原为 Ag 原子, 同时电压也驱动 Br^-和 O^{2-}离子向正极移动, 滞留下溴空位($V_{Br}^{\cdot}$)和氧空位($V_O^{\cdot\cdot}$), 当正电压增大到 Set 电压(2.28 V), 由 Ag、$V_{Br}^{\cdot}$和 $V_O^{\cdot\cdot}$组成的杂化导电细丝连通正负极, 器件转变为低阻态。施加负压后, 随着负压增大, Br^-和 O^{2-}离子回移, Ag 导电细丝断裂, 负压达到 Reset 电压时, 杂化导电细丝断裂, 器件转变为高阻态[19]。

活性电极卤化物钙钛矿阻变器结构中, 钙钛矿层元素不参与导电细丝形成, 金属活性电极元素可以完全主导导电细丝形成。Cu/$MA_3Bi_2I_9$/ITO 器件二次离子质谱(图 2(h))显示钙钛矿阻态转变器件二次 Cu^+离子强度比未转变器件高出数倍, 表明铜元素在钙钛矿中的不同渗透状态导致了导电细丝的形成和断裂, 进而决定了器件阻态转变机理[31]。图 2(i)中 $CsPbI_3$ 钙钛矿层与 Ag 电极为欧姆接触, 与 Pt 电极为肖特基接触。正电压增加促使 Ag 电极氧化溶解($Ag \rightarrow Ag^+ + e^-$), 产生的 Ag^+离子在钙钛矿层通过热激发离子跳跃机制迁移至 Pt 电极, 并被还原成金属银($Ag^+ + e^- \rightarrow Ag$)形成 Ag 导电细丝, 连通器件正负极, 阻变器转变为低阻态[32]。直观的实验观测也证实了卤化物钙钛矿阻变器中导电细丝的形成。$Cs_2AgBiBr_6$ 钙钛矿基阻变器(图 2(j))通过原子力显微镜(AFM)观察到了开(On)态导电细丝(ϕ~30 nm)(图 2(k))[42]。扫描电镜照片(图 2(l))表明器件关(Off)态时 Br 元素和 Ag 元素在钙钛矿薄膜中分布均匀, On 态时 Br 元素和 Ag 元素在 Au 电极聚集, 证实了 Br 元素和 Ag 元素在钙钛矿中的迁移, 这说明电场作用导致 Br^-和 Ag^+离子协同迁移诱导了导电细丝的形成与断裂, 触发阻变器 On/Off 态转变[42]。3D 卤化物钙钛矿阻变器的导电细丝由于器件的电极不同、钙钛矿层组分差异及厚度变化等因素展现出明显不同的特点, 活性电极器件及钙钛矿阻变功能层偏薄的器件以金属导电细丝传导为主, 惰性电极及钙钛矿阻变功能层偏厚的器件以空位导电细丝为主。

1.2 二维结构钙钛矿中的导电细丝机理

二维结构(2D)卤化物钙钛矿具有有机无机层交错的层状结构, 使其具有各向异性电学传输性质和较低的离子迁移效应[44-48]。2D 卤化物钙钛矿基阻变器导电细丝传输机理如图 3 所示。FTO/$[(TZ\text{-}H)_2(PbBr_4)]_n$/Ag (TZ = 1H-1,2,4-triazole)阻变器中 2D 钙钛矿$[(TZ\text{-}H)_2(PbBr_4)]_n$层存在层间有机链形成的缺陷(图 3(ai)), 当正向电压逐渐增大, 注入的载流子填充缺陷(图 3(aii)), 并且驱动 Br^-离子向正极迁移, 在$(PbBr_4)_n^{2n-}$层留下 $V_{Br}^{\cdot}$; 当正向电压增大到 Set 电压, 形成 $V_{Br}^{\cdot}$导电细丝(图 3(aiii))[45]。在阻变器正向电压扫描(图 3(b))过程中, 曲线斜率为 3.25 的阶段为陷阱填充限制模型(TFL)[49], 实现了高阻态向低阻态转变。而且 FTO/$[(TZ\text{-}H)_2(PbBr_4)]_n$/Ag 阻变器在 30~170 ℃范围均表现出典型的双极性阻变存储性能(图 3(c))[45], 说明 2D 钙钛矿阻变器具有优异的耐高温稳定性。

2D 钙钛矿阻变器 Al/$MA_2PbI_2(SCN)_2$/ITO 可以实现高阻态、中阻态、低阻态三态阻变调整(图 3(d))[44]。图 3(e)展示了 Al/MA_2PbI_2 $(SCN)_2$/ITO 阻变器各阶段传导性质, (1)低偏压区的($I \propto V^{0.99}$)填充陷阱载流子热激发电流符合欧姆传导; (2)当电压增大, 钙钛矿层缺陷被逐渐填充, 钙钛矿费米能级提升至接近导带, 实现陷阱填充限制电流(TFLC)$I \propto V^{1.94}$; (3)当电压进一步增大至~1.59 V, 电流 $I \propto V^{1.76}$ 属于空间电荷限制电流(SCLC), 器件实现中阻态; (4)当电压增大到~3.2 V, 电流 $I \propto V^{1.1}$, 器件导电细丝形成, 转变为低阻态。Al/MA_2PbI_2 $(SCN)_2$/ITO 阻变器阻态转变机理如图 3(f)所示, 电压大于 V_{th1}(~1.59 V)时, 钙钛矿膜内的缺陷全部被填充(图 3(fii)), 器件转变为中阻态, 电压大于 V_{th2}(~3.2 V)时, 导电细丝形成(图 3(fiii)), 器

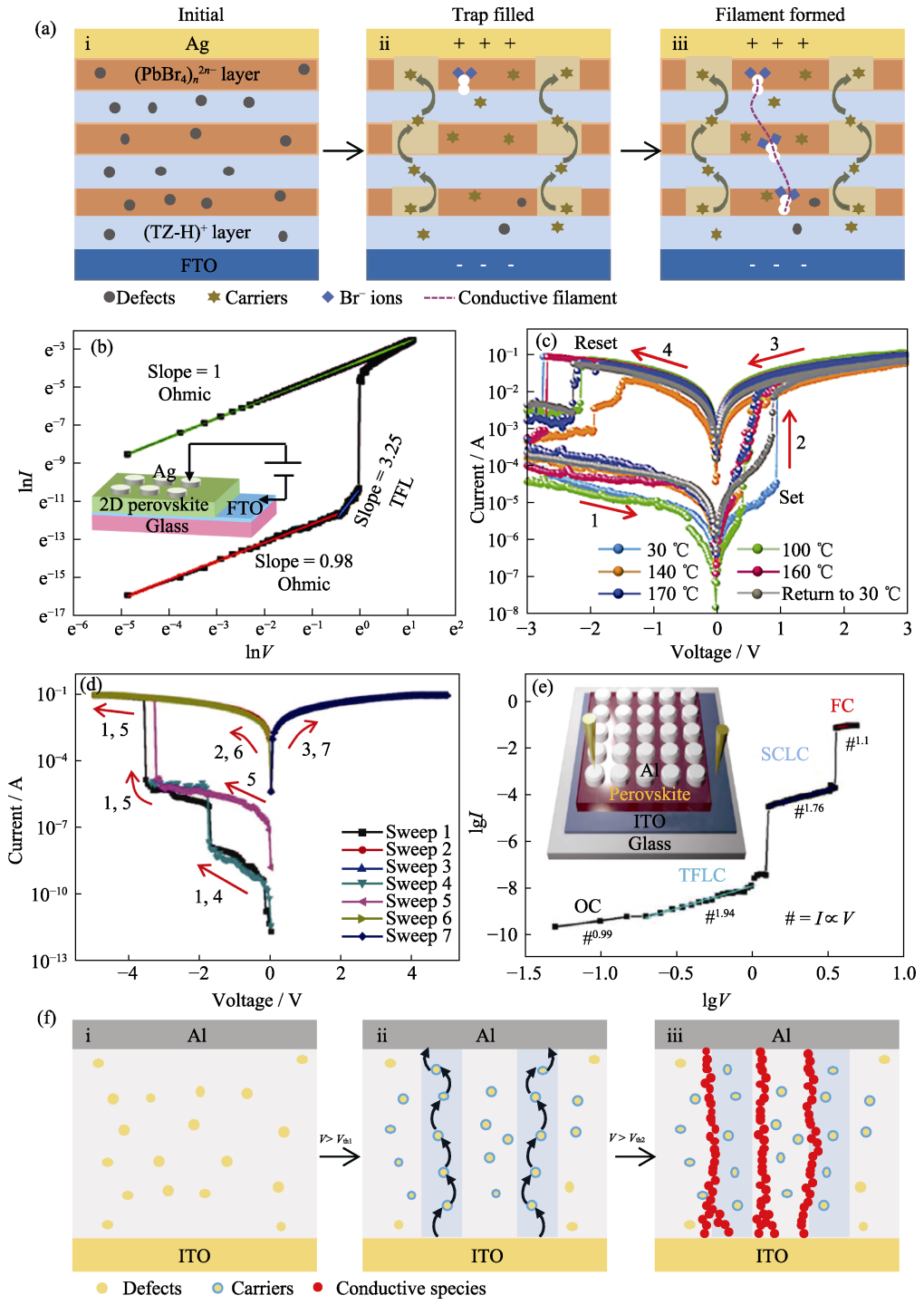

图 3　二维结构(2D)卤化物钙钛矿阻变器的导电细丝[44-45]

Fig. 3　CFs of 2D halide perovskite RS device[44-45]

(a) CFs mechanism of FTO/$[(TZ\text{-}H)_2(PbBr_4)]_n$/Ag device; (b) *I-V* curve with conduction mechanism in semilogarithmic scale under positive-voltage sweep at 30 ℃ with inset showing schematic illustration of FTO/$[(TZ\text{-}H)_2(PbBr_4)]_n$/Ag device structure; (c) *I-V* curves of FTO/$[(TZ\text{-}H)_2(PbBr_4)]_n$/Ag device at different temperatures[45]; (d) Ternary resistive switching *I-V* curves of Al/$MA_2PbI_2(SCN)_2$/ITO device; (e) *I-V* curve with conduction mechanism in semilogarithmic scale with inset showing schematic illustration of Al/$MA_2PbI_2(SCN)_2$/ITO device structure; (f) CFs mechanism of Al/$MA_2PbI_2(SCN)_2$/ITO device[44]. Colorful figures are available on website

件转变为低阻态[44]。所以，2D 卤化物钙钛矿阻变器导电细丝机理与 3D 钙钛矿明显不同。结合两者特点，Lee 等[50]报道了 Ag 作为顶电极的 2D/3D 卤化物钙钛矿异质结结构阻变器，其中 2D 钙钛矿层可以有效控制 Ag 元素迁移和 Ag 导电细丝的断裂，提升了器件的保留特性。2D 卤化物钙钛矿基阻变器在导电细丝形成过程中，出现了显著的载流子填充陷阱阶段，促使其发生阻态转变。

1.3 光对导电细丝的影响

光照可以调控卤化物钙钛矿基光电阻变器导电细丝的生长，提升阻变器性能[51-53]。如图 4(a)所示，$MAPbI_3$ 钙钛矿量子线阻变器 Ag 电极中的 Ag 元素可以与 $MAPbI_3$ 钙钛矿在界面处反应生成 AgI[54]，光照可以促使光敏材料 AgI 分解为 Ag 与 I，并且光生电子与电场负极注入的电子可以增强 Ag^+离子的还原性能，产生额外的 Ag 导电细丝，增大读取电流值。但是，在阻变器 Reset 过程中，光辅助 Ag 导电细丝断裂需要更高的负压[51]。最近报道的柔性云母/AgNWs@AZO/PEDOT:PSS/$CsPbBr_3$/Ag 阻变器，其在亮态下开关比为 10^3，约为暗态的 10 倍，并且具有更佳的阻变稳定性(图 4(b))，证明了光对器件阻变性能的调控作用[52]。开尔文探针原子力显微镜(KPFM)形貌与表面电势图 4(c1~c4)表明光照并不改变卤化物钙钛矿形貌，但是光生载流子显著提高了卤化物钙钛矿表面电势。图 4(d)展示了亮态下柔性云母/AgNWs@AZO/PEDOT:PSS/$CsPbBr_3$/Ag(NWs: nanowires; AZO: aluminum-doped zinc oxide)阻变器 Ag、$V_{Br}^{\cdot}$ 杂化导电细丝的形成与断裂过程，正压增大使 Ag^+离子向负极迁移，而驱动 Br^-离子向正极迁移留下 $V_{Br}^{\cdot}$。光生电子与电场注入电子将 Ag^+离子还原为 Ag 原子，Ag 原子与 $V_{Br}^{\cdot}$ 形成杂化导电细丝连通正负极，器件转变为低阻态(图 4(d Ⅰ~dⅢ))。施加负压电场后，Ag 原子与 $V_{Br}^{\cdot}$ 转为 Ag^+离子与 Br^-离子，导电细丝断裂，器件转变为高阻态(图 4(dⅣ))[52]。

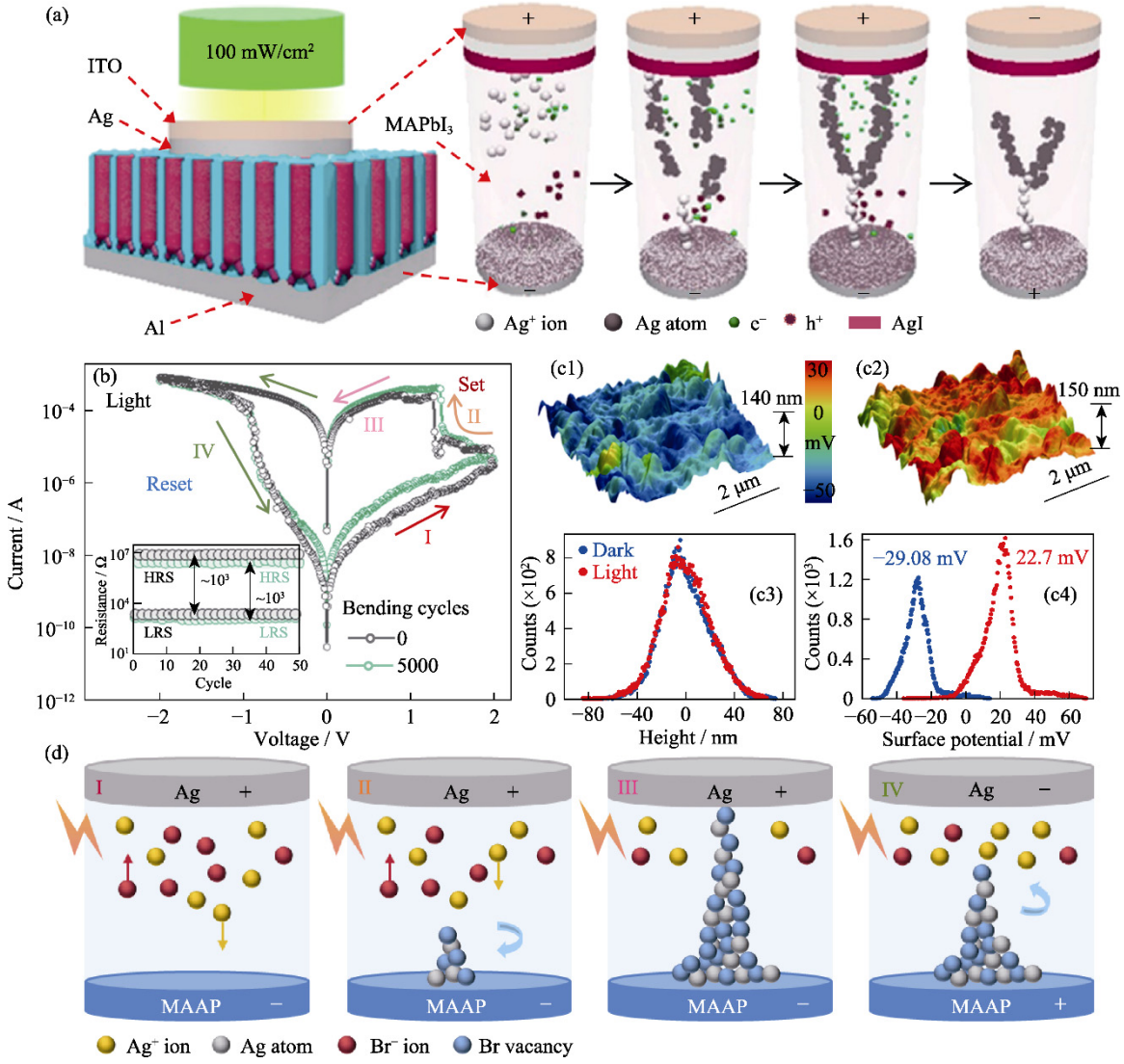

图 4 光照下钙钛矿阻变器的导电细丝[51-52]

Fig. 4 CFs of perovskite RS device under light illumination[51-52]

(a) CFs formation and dissolution of ITO/Ag/$MAPbI_3$ quantum wires/Al device under light illumination[51]; (b) Dynamic bending fatigue *I-V* curves of mica/AgNWs@AZO/PEDOT:PSS/$CsPbBr_3$ device under light illumination; (c) Three-dimensional tomography images of PEDOT: PSS/$CsPbBr_3$ nanocrystal overlaid by Kelvin-probe force microscopy (KPFM) signals under (c1) dark condition and (c2) light illumination, and statistical variations of (c3) height and (c4) surface potential from Figs. (c1, c2); (d) Hybrid filaments formation and dissolution of mica/AgNWs@AZO/PEDOT:PSS/$CsPbBr_3$ device under light illumination[52]. PEDOT: Poly(3,4-ethylenedioxythiophene); PSS: Poly(styrenesulfonate). Colorful figures are available on website

Wu 等[55]也报道了光照调控 $V_I^{\cdot}$ 迁移进而影响阻变突触 Ag/$CH_3NH_3PbI_3$/ITO 器件导电细丝的形成与断裂，实现低电压输入下光可调的突触功能。所以光照可以通过调控卤化物钙钛矿阻变器导电细丝的形成和断裂，增强其性能可靠性[56-57]。Siddik 等[58]报道了光照诱导 Al/FAPbBr$_3$/ITO 阻变器中 Br^-离子迁移有利于形成金属与卤素空位导电细丝，进而影响器件的阻态转变性能。Zheng 等[59]报道了光照不仅可以促进阻变器 Ag/$(PEA)_2PbI_4$/ITO 形成 Ag 导电细丝，而且还可以实现光控的阻变器多阻态存储。光电双控钙钛矿阻变器，使其展现出更丰富的阻变特性，广泛应用于机器视觉与神经网络等领域。

2　卤化物钙钛矿阻变器能级匹配

阻变器中卤化物钙钛矿功能层费米能级和其他结构层功函数不同，其能级匹配会导致界面势垒，影响器件的阻变性能[60-66]。图 5(a)展示了 Ag/PMMA@CsPbI$_3$/FTO(PMMA: polymethylmethacrylate)阻变结构能级匹配，由于电极与 PMMA@CsPbI$_3$ 接触的费米能级对齐效应，PMMA@CsPbI$_3$ 与 Ag 及 FTO 界面处存在由界面指向 PMMA@CsPbI$_3$ 的两个电场耗尽区($E_{bi\text{-}Ag}$ 和 $E_{bi\text{-}FTO}$)，施加偏压与 $E_{bi\text{-}Ag}$ 和 $E_{bi\text{-}FTO}$ 方向相同或相反，对应的耗尽区宽度分别增大或减小，

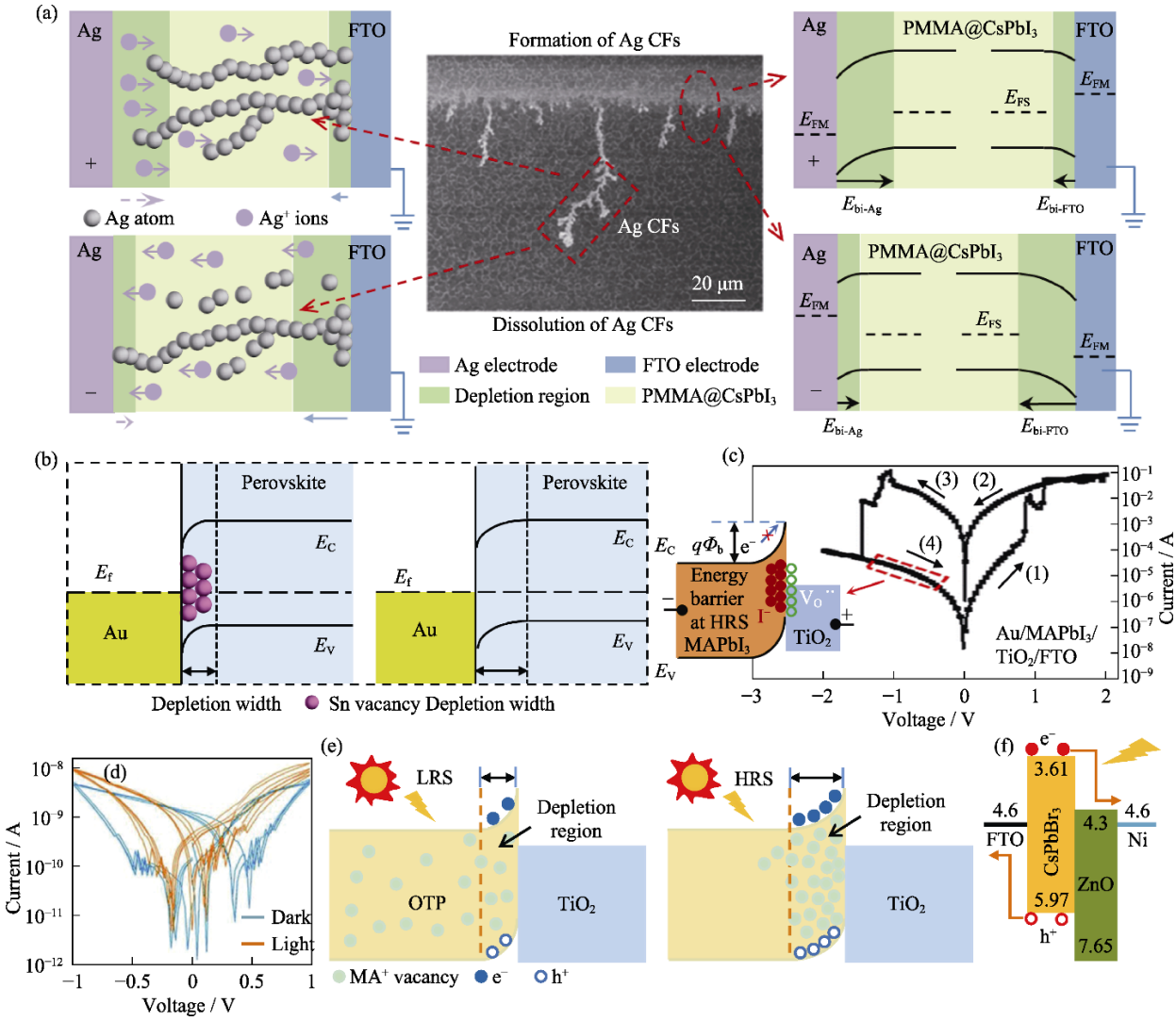

图 5　钙钛矿阻变器的能级匹配[60-64]

Fig. 5　Energy level matching of perovskite RS device[60-64]

(a) Energy level matching and the formation and dissolution of corresponding CFs of Ag/PMMA@CsPbI$_3$/FTO device[60]; (b) Depletion width varied in p-type perovskite CsSnI$_3$ layer due to Sn vacancies under an electric field[61]; (c) Schottky barrier formed at MAPbI$_3$/TiO$_2$ interface and resulting asymmetry *I-V* curve of Au/MAPbI$_3$/TiO$_2$/FTO device[62]; (d) RS loops of Al/$Cs_{0.05}(FA_xMA_{1-x})_{0.95}PbI_yBr_{3-y}$/TiO$_2$/FTO structure under dark condition and light illumination; (e) Depletion region at $Cs_{0.05}(FA_xMA_{1-x})_{0.95}PbI_yBr_{3-y}$/TiO$_2$ interface in low resistance state (LRS) and high resistance state (HRS) under illumination[63]; (f) Light-induced RS behaviours of Ni/ZnO/CsPbBr$_3$/FTO device[64]. Colorful figures are available on website

同时, 也分别对应了导电细丝的形成和断裂[60]。一般情况下, 阻变器一个电极与功能层接触界面为欧姆接触, 另一电极与功能层接触界面为肖特基接触, 肖特基势垒的变化会导致阻态切换[67]。Au 电极与 P 型钙钛矿 $CsSnI_3$ 能级匹配会出现肖特基势垒, 如图 5(b)所示, 施加正向电压, Sn 空位在界面处积累导致对应于肖特基势垒的耗尽区宽度减小, 电场提供的电子容易通过势垒, 阻态逐渐转变为低阻态。施加负压, 界面处 Sn 空位减少, 耗尽区宽度增大, 诱导器件阻态转变为高阻态[61]。另外, Kim 等[68]报道了通过改变阻变器卤化物钙钛矿材料的能带及其引起的能带弯曲可以控制钙钛矿界面处肖特基势垒高度。利用载流子传输层中的离子空位或缺陷也可以调控界面屏障, 图 5(c)展示了电场驱动 TiO_2 中的 $V_O^{\cdot\cdot}$ 吸引 I^-离子在 $MAPbI_3/TiO_2$ 界面处积累, 形成肖特基势垒, 抑制了电子由卤化物钙钛矿向 TiO_2 传输, 并且阻碍 $V_I^{\cdot}$ 导电细丝形成, Au/$MAPbI_3$/TiO_2/FTO 阻变器表现出不对称的阻变行为[62]。配置有 PEDOT:PSS 层的阻变器在 Set 过程中, PEDOT:PSS/钙钛矿界面接触处, PEDOT:PSS 对离子的钉扎作用使载流子更容易越过界面肖特基屏障[69-70]。同样由能级匹配导致的内建电场, 如 ITO/$MASnBr_3$/Au 器件中 Br^-离子和 $V_{Br}^{\cdot}$迁移产生的内部电场耗尽层, 会导致 p-i-n 结, 进而实现阻变电容器件的多级信息存储[71]。

调控光生电子空穴对对肖特基势垒的作用, 可以获得优异的 $CH_3NH_3PbI_{3-x}Cl_x$ 钙钛矿基光电阻变器能级匹配, 提高光电阻态转变性能[72]。图 5(d)展示了光照下 Al/$Cs_{0.05}(FA_xMA_{1-x})_{0.95}PbI_yBr_{3-y}$ (CsFAMAPbIBr)/TiO_2/FTO 阻变器的性能。由于光电流可以通过 CsFAMAPbIBr/TiO_2 界面屏障, 因此高阻态和低阻态电流均增大, 但是, 高阻态电流增加幅度更大, 导致阻变特征曲线迟滞回路变窄。产生这种现象的原因是光照对高阻态 CsFAMAPbIBr/TiO_2 界面耗尽区的调控作用比低阻态更明显[63,73], 如图 5(e)所示。$CsPbBr_3$ 与 ZnO 的能级排布在界面处可以形成异质结, 如图 5(f)所示, 异质结处的内建电场可以在无偏压下分离光生载流子, 同时, ZnO 的价导带低保证了有效提取和传输电子空穴, 因此光控可以实现低偏压条件下 FTO/$CsPbBr_3$/ZnO/Ni 器件的阻态转变行为[64]。卤化物钙钛矿阻变器界面势垒的变化会导致阻态切换, 并且阻态切换一般发生在器件界面处, 因此能级匹配是形成导电细丝的关键条件。

3 卤化物钙钛矿基光电阻变器的应用

卤化物钙钛矿基光电阻变器主要应用于人工突触模拟[74-79]、存储[30-31,80-83]、逻辑运算[84-86]和存算一体/存内运算[87]等方面研究。阻变器的模拟人工突触功能可以实现仿生应用, 在类脑计算及人工视觉神经系统应用中展现出了卓越的性能[88-89], 特别是, 卤化物钙钛矿阻变器应用于人工神经网络系统, 既可以实现长短程记忆分类存储, 又可以利用其光电双控特性模拟视觉神经系统进行准确识别成像[90-91]。

图 6(a)展示了 $CsPbBr_3$ 量子点和碳纳米管作为转换层的光晶体管组成的传感器阵列, 通过调控光脉冲数量和光脉冲能量密度, 可以模拟人类视觉系统, 熟悉面孔成像比偶尔出现的陌生面孔成像更清晰[92]。而基于 $MAPbI_3$ 钙钛矿的突触晶体管模拟生物突触, 如图 6(b)所示, 实现了短期记忆转变为长期记忆, 并且模拟了不同情绪状态下基于短期记忆的视觉学习和存储[79]。还可以将卤化物钙钛矿阻变器整合到人工神经网络系统, 图 6(c)展示了具有典型阻变特征的 $AgBiI_4$ 钙钛矿人工突触组建的生物触觉感知系统, 压力信号作用于 $AgBiI_4$ 钙钛矿人工突触, 使其电阻态发生改变并且被底电极的后突触电流获取, 紧接着电流输入人工神经网络进行识别[93]。除了人工仿生应用外, 卤化物钙钛矿阻变器光电双控阻态切换存储是其另一重要应用[12]。阻变器 Ag/$SrTiO_3$/$CsPbBr_3$/Au(图 6(d))实现了光电探测、存储、光存储三种工作模式, 如图 6(e)所示, 电压 V_3 是阻变器的击穿电压; 当电压 $V > V_2$ 时, 由于强电场容易触发导电细丝的形成, 使阻变器实现存储功能; 当电压 $V_1 < V < V_2$ 时, 阻变器在电场和光照共同作用下可以实现光存储功能; 当电压 $V < V_1$ 时, 在弱电场作用下, 光开关导致了光电流, 使阻变器可以实现光电探测功能[83]。利用阻变器集成结构, 设计高密度钙钛矿光电阻变器存储系统, 图 6(f, g)展示了 Al@$MAPbI_3$/Al 纤维交叉阻变器及其组成的交叉阵列穿戴器件, 其在纤维直径和内部纤维空间减小的情况下, 显著提升了数据存储密度[30]。

调整和输入电脉冲和光脉冲信号还可以实现卤化物钙钛矿基光电阻变器的逻辑运算功能[72]。图 6(h)展示了 $CH_3NH_3SnCl_3$ 钙钛矿基阻变器通过调控输入电压脉冲信号可以实现逻辑“OR”和逻辑“AND”计算[86]。在此基础上, 利用钙钛矿阻变器集成系统可以进一步实现随机逻辑运算, 提高数据安全性。图 6(i)展示了 PrPyr[PbI_3]基阻变器交叉系统作为可重构的物理不可克隆函数, 通过器件系统单次 Reset 重新配置后, 实现了颜色表和数码盘的显著差异性变化, 解决了传统硬件安全解决方案固有的局限性,

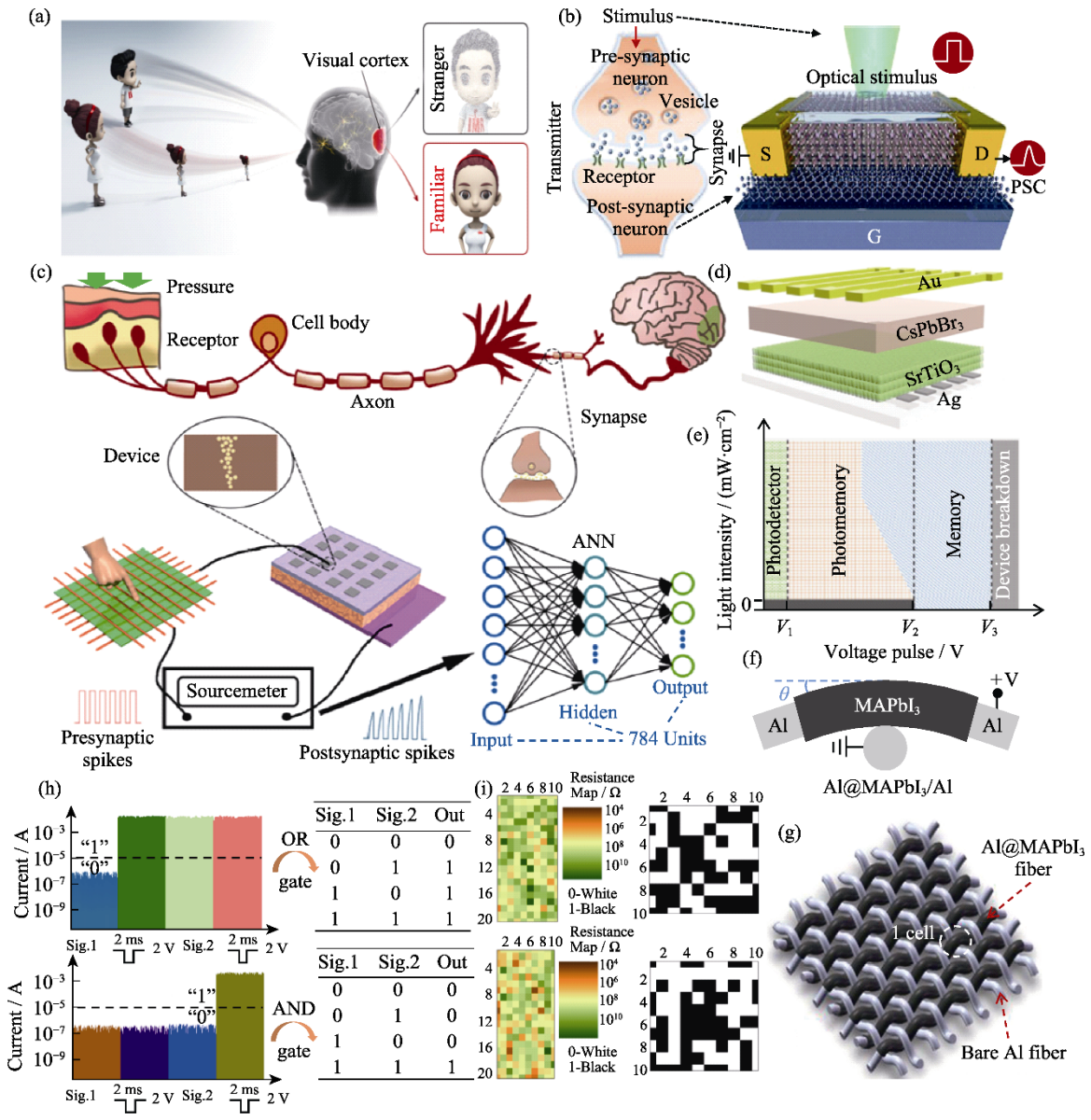

图 6　钙钛矿阻变器的应用[24,30,79,83,86,92-93]

Fig. 6　Application of perovskite-based RS devices[24,30,79,83,86,92-93]

(a) $CsPbBr_3$ quantum dots based phototransistor emulating human visual systems[92]; (b) $MAPbI_3$ based synaptic transistor emulating a biological synapse[79]; (c) $AgBiI_4$ used in artificial sensory neuron system emulating biological tactile sensing system[93]; (d) Schematic illustration of Ag/$SrTiO_3$/$CsPbBr_3$/Au device structure; (e) Photodetector, photomemory, memory mode and breakdown of Ag/$SrTiO_3$/$CsPbBr_3$/Au device[83]; (f, g) Schematic illustration of woven fibrous crosspoint RS devices with the architecture of Al@$MAPbI_3$/Al[30]; (h) Al/$CH_3NH_3SnCl_3$/polyvinyl alcohol/ITO/PET devices achieving logic "OR" and "AND" gate[86]; (i) Physical unclonable functions (memPUFs) of PrPyr[PbI_3] RS devices[24]. PrPyr[PbI_3]: Propyl pyridinium lead iodide

进而阻止机器学习攻击[24]。单一卤化物钙钛矿阻变器及其集成系统可以将逻辑运算与人工突触模拟、存算一体等组合，实现更丰富的功能。Hao 等[25]报道了 $Cs_2AgSbBr_6$ 基阻变仿生器件不但实现了典型的仿生突触行为和学习记忆加强模拟,而且利用输入两种不同波长光脉冲信号，完成了逻辑"OR"和逻辑"AND"计算。Li 等[26]报道了 $CsBi_3I_{10}$ 钙钛矿/碳纳米管基的光电晶体管单电子器件，实现了仿生模拟、存算一体多功能融合。对于阻变器来说，高电阻开关比以及其性能稳定性是其实现应用的重要条件[94-97]，卤化物钙钛矿阻变器高的电阻开关比(超过 10^6)，以及调整电极工程、界面工程、前驱体组分进一步提升器件的稳定性[18,32,98]，使得卤化物钙钛矿基阻变器的多功能商业应用具有广阔的前景。

4　结论与展望

本文从 3D 和 2D 卤化物钙钛矿光电阻变机理出发，详细分析了钙钛矿中 B 位金属、X 位的卤族空位、活性电极金属形成的导电细丝，以及在光电双控

下, 2D 钙钛矿出现的三种阻态及显著的载流子填充陷阱阶段; 讨论了卤化物钙钛矿阻变器界面肖特基势垒形成的能级匹配是高效阻变器的关键因素; 细致分析了光照和电场既可以影响导电细丝的形成和断裂, 又可以改变卤化物钙钛矿层与其它结构层的能级匹配界面势垒的机理, 实现卤化物钙钛矿阻变器的光电双功能调控。然而, 当前光电钙钛矿阻变的研究集中于器件结构本身, 缺少针对光电阻变器信号输出与人工智能结合的整体系统, 也忽视了钙钛矿光电阻变器中导电细丝、能级匹配等机制与智能信号之间的关联。下一步研究将侧重于仿生突触模拟、数据存储和逻辑运算等, 发展可穿戴和智能化薄膜阻变器。光电卤化物钙钛矿阻变器将对大数据和人工智能发展产生深远影响。

参考文献:

[1] WANG S Y, LIU L, GAN L R, *et al.* Two-dimensional ferroelectric channel transistors integrating ultra-fast memory and neural computing. *Nature Communications*, 2021, **12:** 53.

[2] ZHANG B, CHEN W L, ZENG J M, *et al.* 90% yield production of polymer nano-memristor for in-memory computing. *Nature Communications*, 2021, **12:** 1984.

[3] DUBOST V, CREN T, VAJU C, *et al.* Resistive switching at the nanoscale in the mott insulator compound $GaTa_4Se_8$. *Nano Letters*, 2013, **13(8):** 3648.

[4] GAO S, SONG C, CHEN C, *et al.* Dynamic processes of resistive switching in metallic filament-based organic memory devices. *The Journal of Physical Chemistry C*, 2012, **116(33):** 17955.

[5] YOO E J, KIM J H, SONG J H, *et al.* Resistive switching characteristics of the Cr/ZnO/Cr structure. *Journal of Nanoscience and Nanotechnology*, 2013, **13(9):** 6395.

[6] REN S X, LI Z H, LIU X M, *et al.* Oxygen migration induced effective magnetic and resistive switching boosted by graphene quantum dots. *Journal of Alloys and Compounds*, 2021, **863:** 158339.

[7] REN S X, LI Z H, TANG L H, *et al.* Conduction response in highly flexible nonvolatile memory devices. *Advanced Electronic Materials*, 2020, **6(5):** 2000151.

[8] KANG K J, HU W, TANG X S. Halide perovskites for resistive switching memory. *The Journal of Physical Chemistry Letters*, 2021, **12(48):** 11673.

[9] CHUA L O. Memristor-the missing circuit element. *IEEE Transactions on Circuit Theory*, 1971, **18(5):** 507.

[10] STRUKOV D B, SNIDER G S, STEWART D R, *et al.* The missing memristor found. *Nature*, 2008, **453(7191):** 80.

[11] CHUA L. If it's pinched it's a memristor. *Semiconductor Science and Technology*, 2014, **29(10):** 104001.

[12] ZHANG C, LI Y, MA C L, *et al.* Recent progress of organic-inorganic hybrid perovskites in RRAM, artificial synapse, and logic operation. *Small Science*, 2022, **2(2):** 2100086.

[13] REN S X, YANG Z, AN S L, *et al.* High-efficiency photoelectric regulation of resistive switching memory in perovskite quantum dots. *Acta Physico-Chimica Sinica*, 2023, **3(9):** 2301033.

[14] YOO E J, LYU M, YUN J H, *et al.* Resistive switching behavior in organic-inorganic hybrid $CH_3NH_3PbI_{3-x}Cl_x$ perovskite for resistive random access memory devices. *Advanced Materials*, 2015, **27(40):** 6170.

[15] LIU Q, GAO S, XU L, *et al.* Nanostructured perovskites for nonvolatile memory devices. *Chemical Society Reviews*, 2022, **51(9):** 3341.

[16] LAI H J, ZHOU Y, ZHOU H B, *et al.* Photoinduced multi-bit nonvolatile memory based on a van der Waals heterostructure with a 2D-perovskite floating gate. *Advanced Materials*, 2022, **34(19):** 2110278.

[17] MA F M, ZHU Y B, XU Z W, *et al.* Optoelectronic perovskite synapses for neuromorphic computing. *Advanced Functional Materials*, 2020, **30(11):** 1908901.

[18] DI J Y, DU J H, LIN Z H, *et al.* Recent advances in resistive random access memory based on lead halide perovskite. *InfoMat*, 2021, **3(3):** 293.

[19] LIU X M, REN S X, LI Z H, *et al.* Flexible transparent high-efficiency photoelectric perovskite resistive switching memory. *Advanced Functional Materials*, 2022, **32(38):** 2202951.

[20] PARK H L, LEE T W. Organic and perovskite memristors for neuromorphic computing. *Organic Electronics*, 2021, **98:** 106301.

[21] XUE Z Y, XU Y C, JIN C X, *et al.* Halide perovskite photoelectric artificial synapses: materials, devices, and applications. *Nanoscale*, 2023, **15(10):** 4653.

[22] FANG Y T, ZHAI S B, CHU L, *et al.* Advances in halide perovskite memristor from lead-based to lead-free materials. *ACS Applied Materials & Interfaces*, 2021, **13(15):** 17141.

[23] THIEN G S H, AB RAHMAN M, YAP B K, *et al.* Recent advances in halide perovskite resistive switching memory devices: a transformation from lead-based to lead-free perovskites. *ACS Omega*, 2022, **7(44):** 39472.

[24] JOHN R A, SHAH N, VISHWANATH S K, *et al.* Halide perovskite memristors as flexible and reconfigurable physical unclonable functions. *Nature Communications*, 2021, **12:** 3681.

[25] HAO D D, LIU D P, ZHANG J Y, *et al.* Lead-free perovskites-based photonic synaptic devices with logic functions. *Advanced Materials Technologies*, 2021, **6(12):** 2100678.

[26] LI M, XIONG Z Y, SHAO S S, *et al.* Multimodal optoelectronic neuromorphic electronics based on lead-free perovskite-mixed carbon nanotubes. *Carbon*, 2021, **176:** 592.

[27] ABBAS G, HASSAN M, KHAN Q, *et al.* A low power-consumption and transient nonvolatile memory based on highly dense all-inorganic perovskite films. *Advanced Electronic Materials*, 2022, **8(9):** 2101412.

[28] LIU B L, LAI J N, WU D F, *et al.* High-performance resistive random access memories based on two-dimensional $HAPbI_4$ organic-inorganic hybrid perovskite. *The Journal of Physical Chemistry Letters*, 2022, **13(33):** 7653.

[29] LIN Q Q, HU W, ZANG Z G, *et al.* Transient resistive switching memory of $CsPbBr_3$ thin films. *Advanced Electronic Materials*, 2018, **4(4):** 1700596.

[30] SHU P, CAO X F, DU Y Q, *et al.* Resistive switching performance of fibrous crosspoint memories based on an organic-inorganic halide perovskite. *Journal of Materials Chemistry C*, 2020, **8(37):** 12865.

[31] PODDAR S, ZHANG Y T, ZHU Y Y, *et al.* Optically tunable ultra-fast resistive switching in lead-free methyl-ammonium bismuth iodide perovskite films. *Nanoscale*, 2021, **13(12):** 6184.

[32] HAN J S, LE Q V, CHOI J, *et al.* Air-stable cesium lead iodide perovskite for ultra-low operating voltage resistive switching. *Advanced Functional Materials*, 2018, **28(5):** 1705783.

[33] ZHENG Y D, LUO F F, RUAN L X, *et al.* A facile fabrication of lead-free Cs_2NaBiI_6 double perovskite films for memory device application. *Journal of Alloys and Compounds*, 2022, **909:** 164613.

[34] LIU Z H, CHENG P P, LI Y F, *et al.* Multilevel halide perovskite

memristors based on optical & electrical resistive switching effects. *Materials Chemistry and Physics*, 2022, **288:** 126393.

[35] LI Y F, CHENG P P, ZHOU L Y, *et al.* Light-induced nonvolatile resistive switching in $Cs_{0.15}FA_{0.85}PbI_{3-x}Br_x$ perovskite-based memristors. *Solid-State Electronics*, 2021, **186:** 108166.

[36] CAO X F, HAN Y Z, ZHOU J K, *et al.* Enhanced switching ratio and long-term stability of flexible RRAM by anchoring polyvinylammonium on perovskite grains. *ACS Applied Materials & Interfaces*, 2019, **11(39):** 35914.

[37] SUN Y M, TAI M Q, SONG C, *et al.* Competition between metallic and vacancy defect conductive filaments in a $CH_3NH_3PbI_3$-based memory device. *The Journal of Physical Chemistry C*, 2018, **122(11):** 6431.

[38] PARAMANIK S, MAITI A, CHATTERJEE S, *et al.* Large resistive switching and artificial synaptic behaviors in layered $Cs_3Sb_2I_9$ lead-free perovskite memory devices. *Advanced Electronic Materials*, 2022, **8(1):** 2100237.

[39] GEORGE T, MURUGAN A V. Improved performance of the Al_2O_3-protected HfO_2-TiO_2 base layer with a self-assembled $CH_3NH_3PbI_3$ heterostructure for extremely low operating voltage and stable filament formation in nonvolatile resistive switching memory. *ACS Applied Materials & Interfaces*, 2022, **14(45):** 51066.

[40] PARK Y, LEE J S. Metal halide perovskite-based memristors for emerging memory applications. *The Journal of Physical Chemistry Letters*, 2022, **13(24):** 5638.

[41] PAUL T, SARKAR P K, MAITI S, *et al.* Multilevel programming and light-assisted resistive switching in a halide-tunable all-inorganic perovskite cube for flexible memory devices. *ACS Applied Electronic Materials*, 2020, **2(11):** 3667.

[42] CHENG X F, QIAN W H, WANG J, *et al.* Environmentally robust memristor enabled by lead-free double perovskite for high-performance information storage. *Small*, 2019, **15(49):** 1905731.

[43] SUN Y M, SONG C, YIN J, *et al.* Guiding the growth of a conductive filament by nanoindentation to improve resistive switching. *ACS Applied Materials & Interfaces*, 2017, **9(39):** 34064.

[44] CHENG X F, HOU X, ZHOU J, *et al.* Pseudohalide-induced 2D $(CH_3NH_3)_2PbI_2(SCN)_2$ perovskite for ternary resistive memory with high performance. *Small*, 2018, **14(12):** 1703667.

[45] SONG K Y, CHEN B J, LIN X L, *et al.* Thermal enhanced resistive switching performance of <100>-oriented perovskite $[(TZ\text{-}H)_2(PbBr_4)]_n$ with high working temperature: a triazolium/$(PbBr_4)_n^{2n-}$ interfacial interaction insight. *Advanced Electronic Materials*, 2022, **8(11):** 2200537.

[46] WANG Z P, LIN Q Q, CHMIEL F P, *et al.* Efficient ambient-air-stable solar cells with 2D-3D heterostructured butylammonium-caesium-formamidinium lead halide perovskites. *Nature Energy*, 2017, **2(9):** 17135.

[47] LIU Y C, YE H C, ZHANG Y X, *et al.* Surface-tension-controlled crystallization for high-quality 2D perovskite single crystals for ultrahigh photodetection. *Matter*, 2019, **1(2):** 465.

[48] DI J Y, LIN Z H, SU J, *et al.* Two-dimensional $(C_6H_5C_2H_4NH_3)_2PbI_4$ perovskite single crystal resistive switching memory devices. *IEEE Electron Device Letters*, 2021, **42(3):** 327.

[49] BHARATHI M, BALRAJ B, SIVAKUMAR C, *et al.* Effect of Ag doping on bipolar switching operation in molybdenum trioxide (MoO_3) nanostructures for non-volatile memory. *Journal of Alloys and Compounds*, 2021, **862:** 158035.

[50] LEE S M, KIM H, KIM D H, *et al.* Tailored 2D/3D halide perovskite heterointerface for substantially enhanced endurance in conducting bridge resistive switching memory. *ACS Applied Materials & Interfaces*, 2020, **12(14):** 17039.

[51] PODDAR S, ZHANG Y T, GU L L, *et al.* Down-scalable and ultra-fast memristors with ultra-high density three-dimensional arrays of perovskite quantum wires. *Nano Letters*, 2021, **21(12):** 5036.

[52] ZHANG G L, XU Y Q, YANG S, *et al.* Robust mica perovskite photoelectric resistive switching memory. *Nano Energy*, 2023, **106:** 108074.

[53] ZHAO X N, WANG Z Q, LI W T, *et al.* Photoassisted electroforming method for reliable low-power organic-inorganic perovskite memristors. *Advanced Functional Materials*, 2020, **30(17):** 1910151.

[54] KATO Y, ONO L K, LEE M V, *et al.* Silver iodide formation in methyl ammonium lead iodide perovskite solar cells with silver top electrodes. *Advanced Materials Interfaces*, 2015, **2(13):** 1500195.

[55] HAM S, CHOI S, CHO H, *et al.* Photonic organolead halide perovskite artificial synapse capable of accelerated learning at low power inspired by dopamine-facilitated synaptic activity. *Advanced Functional Materials*, 2019, **29(5):** 1806646.

[56] LIU Z H, CHENG P P, KANG R Y, *et al.* Photo-enhanced resistive switching effect in high-performance $MAPbI_3$ memristors. *Advanced Materials Interfaces*, 2023, **10(2):** 2201513.

[57] ROGDAKIS K, LOIZOS M, VISKADOUROS G, *et al.* Memristive perovskite solar cells towards parallel solar energy harvesting and processing-in-memory computing. *Materials Advances*, 2022, **3(18):** 7002.

[58] SIDDIK A, HALDAR P K, DAS U, *et al.* Organic-inorganic $FAPbBr_3$ perovskite based flexible optoelectronic memory device for light-induced multi level resistive switching application. *Materials Chemistry and Physics*, 2023, **297:** 127292.

[59] ZHENG Y C, YU D F, LIAN H J, *et al.* Controllable extrinsic ion transport in two-dimensional perovskite films for reproducible, low-voltage resistive switching. *Science China Materials*, 2023, **66:** 2383.

[60] XU J, WU Y H, LI Z Z, *et al.* Resistive switching in nonperovskite-phase $CsPBI_3$ film-based memory devices. *ACS Applied Materials & Interfaces*, 2020, **12(8):** 9409.

[61] HAN J S, LE Q V, CHOI J, *et al.* Lead-free all-inorganic cesium tin iodide perovskite for filamentary and interface-type resistive switching toward environment-friendly and temperature-tolerant nonvolatile memories. *ACS Applied Materials & Interfaces*, 2019, **11(8):** 8155.

[62] LEE S, WOLFE S, TORRES J, *et al.* Asymmetric bipolar resistive switching of halide perovskite film in contact with TiO_2 layer. *ACS Applied Materials & Interfaces*, 2021, **13(23):** 27209.

[63] WANG S X, DONG X Q, XIONG Y X, *et al.* CsFAMAPbIBr photoelectric memristor based on ion-migration induced memristive behavior. *Advanced Electronic Materials*, 2021, **7(5):** 2100014.

[64] WU Y, WEI Y, HUANG Y, *et al.* Capping $CsPbBr_3$ with ZnO to improve performance and stability of perovskite memristors. *Nano Research*, 2017, **10(5):** 1584.

[65] SEO J Y, CHOI J, KIM H S, *et al.* Wafer-scale reliable switching memory based on 2-dimensional layered organic-inorganic halide perovskite. *Nanoscale*, 2017, **9(40):** 15278.

[66] MA H L, WANG W, XU H Y, *et al.* Interface state-induced negative differential resistance observed in hybrid perovskite resistive switching memory. *ACS Applied Materials & Interfaces*, 2018, **10(25):** 21755.

[67] SAWA A. Resistive switching in transition metal oxides. *Materials Today*, 2008, **11(6):** 28.

[68] KIM H, CHOI M J, SUH J M, *et al.* Quasi-2D halide perovskites for resistive switching devices with ON/OFF ratios above 10^9. *NPG Asia Materials*, 2020, **12(1):** 21.

[69] DAS U, SARKAR P K, DAS D, *et al.* Influence of nanoscale charge trapping layer on the memory and synaptic characteristics of a novel rubidium lead chloride quantum dot based memristor.

Advanced Electronic Materials, 2022, **8(5):** 2101015.

[70] JOHN R A, YANTARA N, NG Y F, *et al.* Ionotronic halide perovskite drift-diffusive synapses for low-power neuromorphic computation. *Advanced Materials*, 2018, **30(51):** 1805454.

[71] QIAN W H, CHENG X F, ZHAO Y Y, *et al.* Independent memcapacitive switching triggered by bromide ion migration for quaternary information storage. *Advanced Materials*, 2019, **31(37):** 1806424.

[72] ZHOU F C, LIU Y H, SHEN X P, *et al.* Low-voltage, optoelectronic $CH_3NH_3PbI_{3-x}Cl_x$ memory with integrated sensing and logic operations. *Advanced Functional Materials*, 2018, **28(15):** 1800080.

[73] GUAN X W, HU W J, HAQUE M A, *et al.* Light-responsive ion-redistribution-induced resistive switching in hybrid perovskite Schottky junctions. *Advanced Functional Materials*, 2018, **28(3):** 1704665.

[74] LI M Z, GUO L C, DING G L, *et al.* Inorganic perovskite quantum dot-based strain sensors for data storage and in-sensor computing. *ACS Applied Materials & Interfaces*, 2021, **13(26):** 30861.

[75] HUANG X, LI Q Y, SHI W, *et al.* Dual-mode learning of ambipolar synaptic phototransistor based on 2D perovskite/organic heterojunction for flexible color recognizable visual system. *Small*, 2021, **17(36):** 2102820.

[76] HAO J, KIM Y H, HABISREUTINGER S N, *et al.* Low-energy room-temperature optical switching in mixed-dimensionality nanoscale perovskite heterojunctions. *Science Advances*, 2021, **7(18):** eabf1959.

[77] YANG X Y, XIONG Z Y, CHEN Y J, *et al.* A self-powered artificial retina perception system for image preprocessing based on photovoltaic devices and memristive arrays. *Nano Energy*, 2020, **78:** 105246.

[78] YANG J Q, WANG R P, WANG Z P, *et al.* Leaky integrate-and-fire neurons based on perovskite memristor for spiking neural networks. *Nano Energy*, 2020, **74:** 104828.

[79] YIN L, HUANG W, XIAO R L, *et al.* Optically stimulated synaptic devices based on the hybrid structure of silicon nanomembrane and perovskite. *Nano Letters*, 2020, **20(5):** 3378.

[80] YEN M C, LEE C J, LIU K H, *et al.* All-inorganic perovskite quantum dot light-emitting memories. *Nature Communications*, 2021, **12:** 4460.

[81] ERCAN E, LIN Y C, HSU L C, *et al.* Multilevel photonic transistor memory devices based on 1D electrospun semiconducting polymer/perovskite composite nanofibers. *Advanced Materials Technologies*, 2021, **6(8):** 2100080.

[82] VASILOPOULOU M, KIM B S, KIM H P, *et al.* Perovskite flash memory with a single-layer nanofloating gate. *Nano Letters*, 2020, **20(7):** 5081.

[83] GUAN X W, WAN T, HU L, *et al.* A solution-processed all-perovskite memory with dual-band light response and tri-mode operation. *Advanced Functional Materials*, 2022, **32(16):** 2110975.

[84] PEI J X, WU X H, LIU W J, *et al.* Photoelectric logic and *in situ* memory transistors with stepped floating gates of perovskite quantum dots. *ACS Nano*, 2022, **16(2):** 2442.

[85] LIU Q, YUE W J, LI Y, *et al.* Multifunctional optoelectronic random access memory device based on surface-plasma-treated inorganic halide perovskite. *Advanced Electronic Materials*, 2021, **7(7):** 2100366.

[86] SUN Y M, WEN D Z. Logic function and random number generator build based on perovskite resistive switching memory and performance conversion *via* flexible bending. *ACS Applied Electronic Materials*, 2020, **2(2):** 618.

[87] CHEN Q L, ZHANG Y, LIU S Z, *et al.* Switchable perovskite photovoltaic sensors for bioinspired adaptive machine vision. *Advanced Intelligent Systems*, 2020, **2(9):** 2000122.

[88] YAN X B, HE H D, LIU G J, *et al.* A robust memristor based on epitaxial vertically aligned nanostructured $BaTiO_3$-CeO_2 films on silicon. *Advanced Materials*, 2022, **34(23):** 2110343.

[89] PEI Y F, LI Z Q, LI B, *et al.* A multifunctional and efficient artificial visual perception nervous system with Sb_2Se_3/CdS-core/shell (SC) nanorod arrays optoelectronic memristor. *Advanced Functional Materials*, 2022, **32(29):** 2203454.

[90] PARK Y, KIM M K, LEE J S. 2D layered metal-halide perovskite/oxide semiconductor-based broadband optoelectronic synaptic transistors with long-term visual memory. *Journal of Materials Chemistry C*, 2021, **9(4):** 1429.

[91] KIM S J, LEE T H, YANG J M, *et al.* Vertically aligned two-dimensional halide perovskites for reliably operable artificial synapses. *Materials Today*, 2022, **52:** 19.

[92] ZHU Q B, LI B, YANG D D, *et al.* A flexible ultrasensitive optoelectronic sensor array for neuromorphic vision systems. *Nature Communications*, 2021, **12(1):** 1798.

[93] YE H B, LIU Z Y, HAN H D, *et al.* Lead-free $AgBiI_4$ perovskite artificial synapses for a tactile sensory neuron system with information preprocessing function. *Materials Advances*, 2022, **3(19):** 7248.

[94] YAN X B, PEI Y F, CHEN H W, *et al.* Self-assembled networked PbS distribution quantum dots for resistive switching and artificial synapse performance boost of memristors. *Advanced Materials*, 2019, **31(7):** 1805284.

[95] PEI Y F, YAN L, WU Z H, *et al.* Artificial visual perception nervous system based on low-dimensional material photoelectric memristors. *ACS Nano*, 2021, **15(11):** 17319.

[96] YAN X B, YAN H W, LIU G J, *et al.* Silicon-based epitaxial ferroelectric memristor for high temperature operation in self-assembled vertically aligned $BaTiO_3$-CeO_2 films. *Nano Research*, 2022, **15(10):** 9654.

[97] YANG Y, OUYANG J Y, MA L P, *et al.* Electrical switching and bistability in organic/polymeric thin films and memory devices. *Advanced Functional Materials*, 2006, **16(8):** 1001.

[98] YAN K, PENG M, YU X, *et al.* High-performance perovskite memristor based on methyl ammonium lead halides. *Journal of Materials Chemistry C*, 2016, **4(7):** 1375.